PERGAMON

International Journal of Heat and Mass Transfer 43 (2000) 2059–2073

International Journal of HEAT and MASS TRANSFER

www.elsevier.com/locate/ijhmt

A new model for the effective thermal conductivity of packed beds of solid spheroids: alumina in helium between 100 and 500°C

Alan J. Slavin*, Frank A. Londry, Joy Harrison

Department of Physics, Trent University, Peterborough, ON, Canada K9J 7B8

Received 7 March 1999; received in revised form 23 September 1999

Abstract

An analytical model is given for the thermal conductivity of a bed of solid spheroidal particles in static gas, when the conductivity of the solid is substantially greater than that of the gas. It has two fitting parameters, the width and average radius of the narrow gaps that exist between the irregularly shaped particles and which contribute significantly to the thermal conductivity. Since both parameters are physically measurable, the model holds the potential for calculating the thermal conductivity without any adjustable parameters. Agreement is excellent with measurements on alumina particles in helium at 100–500°C up to 100 kPa pressure.

1. Introduction

There is considerable interest in the thermal conductivity of beds of solid spheroids in the presence of a gas. Such beds have been proposed for thermal insulation [1,2] and as the breeder blanket about a fusion reactor [3], and are also of interest as beds for chemical reactions [4] and in drying processes [5].

The present experimental data with alumina spheroids was taken to test new apparatus for measurements on materials of interest in fusion reactors. The data agrees well with earlier results at discrete temperatures [6,7], and a modified form of the apparatus has been used subsequently with lithium zirconate spheres [8].

Numerous analytic models have been developed for calculating the effective thermal conductivity of packed pebble beds in the presence of a static gas. Examples are the models by Hall and Martin [9] referred to as HM, and the model of Zehner, Bauer and Schlünder [10] referred to as ZBS. Three recent evaluations of a number of these models have been carried out by Tsotsas and Martin [11], Fundamenski and Gierszewski [12], and Xu et al. [13]. The first two studies concluded that a modified form of the ZBS model [10] did the best job of describing the experimental data. The third study found serious deficiencies with all three analytic models tested, and concluded that the UCLA two-dimensional, finite-element model [14] gave the most reliable predictions using reasonable parameters. However, none of the analytic models considered in the latter two surveys gave consistent values of the fitting parameters when applied to the present alumina data (finite-element models were not tried). An examination of our data, as discussed below,

* Corresponding author. Tel.: +1-705-748-1289; fax: +1-705-748-1625.

E-mail address: aslavin@trentu.ca (A.J. Slavin).

0017-9310/00/$ - see front matter
PII: S0017-9310(99)00290-2

Nomenclature

a	accommodation coefficient
B	average radius of the area delineated by the points of contact of two spheroids
C_v	heat capacity per molecule at constant volume
C_P	heat capacity per molecule at constant pressure
d	gap between two surfaces confining the gas
D	molecular diameter
f_j	Gaussian weighting factor for the area of a gap of width g_j
g	"inner" gap width in the single-gap model
g_{av}	average "inner" gap width in the multiple-gap model
g_j	average gap width in the jth Gaussian bin
G	total conductance of one cell
G_c	conductance through the contact points between spheroids
G_i	gas conductance through the "inner" gap, of average width g_{av}, between particles
G_{iM}	gas conductance through all the inner gaps, in the multiple-gap model
G_o	gas conductance through the gap outside the area delineated by the points of contact
G_r	conductance between spheres by radiation
G_s	conductance through the solid sphere
h_r	average height of the short-range roughness
j	temperature jump distance at a surface
k	Boltzmann's constant
K_{eff}	effective thermal conductivity of the packed bed
n	molecular number density ($n=P/kT$)
P	gas pressure
Pr	gas Prandtl number
$\dot{Q}$	heat flow in watts
r_1, r_2	radii at which the temperature is measured in determining K_{eff}
r_c	average radius of the area of the contact points between two spheres
R	average radius of a spheroid
R_c	correlation coefficient from a regression analysis
T	temperature in Kelvin
$\bar{v}$	average molecular velocity

Greek symbols

α_c, α_e, α_i, α_o, α_r, α_s	geometrical correction factor for the conductances G_c, G, G_i, G_o, G_r and G_s, respectively
β	factor to correct for the linear term in $[1-\exp(-3\ g/2\lambda)]$ at low values of g/λ
γ	the ratio C_P/C_V
δ	area of direct contact between adjacent spheroids
ϵ	thermal emissivity of alumina
σ	standard deviation of the Gaussian distribution of gap widths
σ_S	Stefan–Boltzmann constant
λ	molecular mean free path
θ	polar angle

led us to the conclusion that long-range surface undulations (as opposed to short-range roughness) will allow two adjacent particles to be in contact at more than the one point normally assumed, resulting in extended areas with gaps between the particles which may be comparable in width to the gas mean free path. Although these areas are typically much smaller than the cross section of the particle, the narrow gap results in a contribution to the thermal conductivity that is often larger than from the gas outside of these gaps.

The ZBS model is a very general one which accommodates a range of particle geometries from spheres to cylinders. It does include a contribution from the narrow gaps, but defines their effective size in terms of the bed porosity in a way which is not easily related to the physical dimensions of the gaps, which can vary dramatically depending on the smoothness of the spheroids. It also includes conduction through the contact between particles by introduction of a "flattening coefficient" ϕ which is essentially the fraction of the spheroid cross-sectional area which is in contact with an adjacent particle. The HM model includes essentially the same expression as in the ZBS model for the evolution of the gaseous thermal conductivity from that at low pressures to that at high pressures, but

does not include the extended narrow gaps. One of the problems with both these models is that, to obtain acceptable fits to experimental data, they require unreasonably large values for the contact area between adjacent particles. For example, Enoeda et al. [15] have fitted their data on several materials using the ZBS and HM models. These fits required contact radii of typically 0.7% of the pebble diameter, which are substantially higher than would be expected from the elastic moduli and the weight of the particle beds. The problem with obtaining reasonable values for the contact area from these models has also been noted by Xu et al. [13], who obtained acceptable fits to beryllium data with a finite element model with the assumption of point contact only.

No analytic model was found that incorporated the narrow gaps satisfactorily, so a new model has been developed. (Adnani et al. [16] and Xu et al. [13] have included local surface roughness in their finite-element analyses, but did not include the longer-range surface undulations.) The new model in its most general form provides a good fit to our experimental alumina data, with relatively few fitting parameters, all of which have clear physical significance and reasonable values. The number of fitting parameters can be reduced to two without significant change in the quality of fit, with both parameters being measurable from the spheroids, in principle. The 2-parameter model also provides an excellent fit to the data reported by Xu et al. [13] for the conductivity of beds of beryllium spheres in the presence of He and N_2 gases, with no fitting parameters in the latter case.

2. Apparatus

The experimental apparatus was a cylinder containing an axial heat source surrounded by the alumina. Thermocouples were imbedded in the alumina at different radial positions to measure temperatures. For this geometry, under steady state conditions and ignoring end effects, the heat flow outwards through a cylindrical surface of radius r and length l is

$$\dot{Q} = -2\pi r l K(T)\frac{\mathrm{d}T}{\mathrm{d}r} \tag{1}$$

where T is the temperature at radial position r and $K(T)$ is the local effective thermal conductivity. Integrating, one obtains a mean effective thermal conductivity K_{eff} between two radial positions r_1 and r_2 at which the temperatures are T_1 and T_2, respectively, with

$$K_{\mathrm{eff}} = \frac{\dot{Q}}{2\pi l}\,\frac{\ln(r_2/r_1)}{T_1 - T_2}. \tag{2}$$

The cell used in these experiments, and sketched in Fig. 1, consisted of a vertical pyrex tube with an inside diameter of 88.9 mm and a wall thickness of 3.18 mm with 150-mm diameter stainless-steel conflat flanges connected to each end through glass-to-metal seals. Overall length of the cell between conflats was 648 mm. (This cell failed by fracture of the pyrex tube as the experiments were being concluded. The tube was replaced by an inconel one for subsequent experiments on lithium zirconate beds [3,8].)

The cell was connected to a 44-liter gas cylinder held at the same pressure as the cell but at room temperature, which acted as a ballast to hold the pressure in the cell essentially constant as the cell temperature was changed. The changes in pressure as the cell (and room) heated were too small to require corrections to the results.

The principal heat source for the cell consisted of resistance wire wound around a hollow mullite rod (IMUL900, Abar-Ipsen of Pecaponia, IL) with outside diameter 19.1 mm and wall thickness 3.18 mm, which was coaxial with the pyrex cylinder. The resistance wire (A1 Kanthal, of resistance 1.119 Ω/m) was positioned uniformly on the mullite rod by means of a spiral groove in the mullite rod, with approximately 350 grooves/m. The thermal conductivity of IMUL900 was given as ranging between 2 and 10 W m^{-1} K^{-1}.

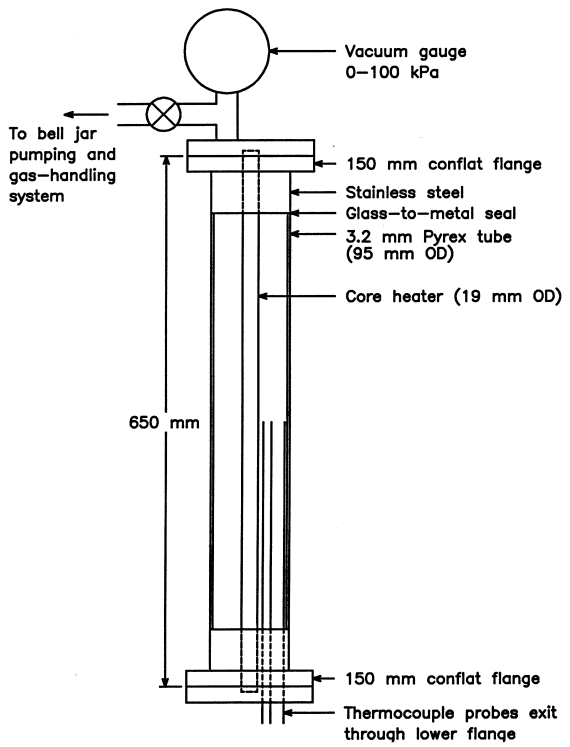

Fig. 1. Cross section of the thermal conductivity cell.

The outside of the cell between the conflat flanges was wrapped with a heavily insulated heater tape, to reduce the radial temperature gradient across the bed. Although the tape was not powered when the pressure of He in the cell was greater than 3 kPa, it did insulate the cell sufficiently well to reduce the overall radial temperature difference by more than 100°C when the temperature at the innermost thermocouple was above 400°C. To minimize the longitudinal temperature gradients across the glass-to-metal seals and reduce axial heat flow within the cell, the upper conflat flange was wrapped with rock-wool insulation to extend the cylinder of insulation above and below the end flanges by about 7 cm. The lower conflat flange and the clamp in which it was held were wrapped with another heavily insulated heater tape.

The electrical power supplied to the axial heater, to the heater tape which wrapped the cell, and to the heater tape which wrapped the base, was adjusted by three variacs. The electrical power dissipated in the axial heater was determined by measuring the ac current and the potential between voltage taps which were welded to the resistance wire 50 mm above and below the longitudinal centre of the axial heater. Voltage taps near the cell centre were used to obviate resistance changes in the heater wire with temperature.

Temperatures inside the cell were measured with type-K thermocouple probes from Omega Engineering. The thermocouple junctions and lead wires were contained within, and electrically insulated (with MgO) from, inconel sheaths whose outside diameter was 0.25 mm. The probes were silver-soldered into hypodermic needles which had been welded into the bottom conflat flange.

Cotton threads were used to hold the thermocouple probes in position while the cell was being filled with the ceramic spheres. When the cell had been filled to the point where the end of a thermocouple probe was only a few millimetres above the level of the alumina, the radial position of the end of the probe relative to the heater core was measured through the pyrex wall using a travelling microscope. Optical distortions due to the curvature of the pyrex tube were shown to be negligible by measuring the positions of the graduations on a scale placed inside the cylinder. The filling of the cell with alumina was then completed and the threads from the thermocouples cut off. In order to minimize the effect of changes in packing density near the walls, the radial positions of the innermost and outermost thermocouples were chosen to allow about 2 sphere diameters between these thermocouples and the axial heater or cell wall, respectively. The cell was always operated for at least 30 min before any measurements were taken, to allow time for vibrations from the pumping system to increase the cell packing.

Six thermocouple probes were installed inside the cell. Three of these, denoted $M1$, $M2$ and $M3$, were located in the mid-plane of the cell, with $M1$ nearest the heater, $M3$ nearest the cell wall, and $M2$ roughly halfway between $M1$ and $M3$. In order to check for longitudinal variations in temperature, $B1$ and $B3$ were located 50 mm below the mid-plane, while $T1$ was located 50 mm above the mid-plane; B1 and $T1$ were nominally at the same radial position as $M1$, and $B3$ as $M3$.

The amount of He gas in the cell and ballast was adjusted to give a desired pressure, and then not changed until the thermal conductivity was measured over the full range of temperature. The thermal conductivity of the beds was measured for pressures of roughly 100, 40, 11, 5 and 0 ($<1\times10^{-5}$) kPa. The pressure was measured with a Matheson gauge, model 63-5601, which reads from 0 to 100 kPa with a resolution of 0.2 kPa. During the experiments it was discovered that the pressure indicated by the gauge varied as a function of barometric pressure. Therefore, after completion of experiments, the gauge was calibrated against a Baratron capacitance manometer (type 122A, model 5000). The correct pressure was found to be given within 0.2 kPa by

$$P = 1.008P_{\mathrm{M}} + 1.025(P_{\mathrm{B}} - 100.5) \tag{3}$$

where P_{M} is the reading from the Matheson gauge and P_{B} is the barometric pressure. All pressures reported here have been corrected in this manner, using values of barometric pressure recorded at the time of the experiment or obtained from local weather records.

3. The alumina spheroids

Experiments were carried out on two different ranges of sphere size, and of slightly different chemical composition. Physical characteristics of these spheres are given in Table 1, as provided by the supplier, US Stoneware, Mahwah, NJ, except for the average diameter and ratio of diameters which were measured in our laboratory.

Also appearing in Table 1 is the packing fraction for the spheres. This number was measured by comparing the mass and volume of a quantity of spheres contained in a vessel, with dimensions similar to those of the cell, with the values of specific gravity supplied by US Stoneware. The before-tapping packing fraction was obtained by simply pouring the spheres into the vessel to a predetermined level. The after-tapping value was determined after the vessel had been repeatedly tapped against the floor until the level of the spheres stabilized (about 50 or 60 taps). The tapping compressed the volume of the smaller spheres by 10.3% and the volume of the larger spheres by 5.5%. When

Table 1
Physical characteristics of the alumina spheroids

Nominal diameter		1 mm	3 mm
Range of sphere diameters (mm)		0.85–1.40	2.36–3.35
Average diameter (mm)		0.936 ± 0.06	2.70 ± 0.17
Ratio of perpendicular diameters		1.06 ± 0.06	1.04 ± 0.04
Chemical composition (%)	Al_2O_3	96.34	85–90
	SiO_2	2.75	8–10
	MgO	0.6	1.5
Specific gravity		3.64	3.48
Porosity (%)		0.0	0.0
Packing fraction (%)	Before tapping	51.4	55.0
	After tapping	56.7	58.0

examined under a microscope the smaller spheres appeared to be less spheroidal than the larger ones, which may have affected the packing density. No measurements were taken to determine the packing fraction of the spheres under the actual experimental conditions, but it is expected that vibrations from the pumping system and thermal cycling would increase the packing fraction to a value near the after-tapping value. The diameters of about 100 spheroids from each group were measured with calipers, and the ratio obtained of two, randomly selected, perpendicular diameters for each spheroid to give a rough measure of oblateness and/or long-range irregularities. These values are also recorded in Table 1. The uncertainties given represent one standard deviation throughout this paper.

4. Experimental results

The thermal conductivity data for the 1-mm spheres are displayed as the solid points in Fig. 2 which shows the mean effective thermal conductivity between thermocouples $M1$ and $M3$ as a function of the average temperature of $M1$ and $M3$. The corresponding results for the 3-mm spheres are given in Fig. 3. The open points represent the work of other researchers and the lines are theoretical fits to be discussed later. The experimental results of Sordon [7] for alumina spheres with diameters of 1-mm, 2-mm and 4-mm in 100 kPa of helium, obtained by a similar technique, are included in Figs. 2 and 3. Each of Sordon's data points is an average of results obtained at two different axial positions. Fig. 2 also shows the results of McElroy et al. [6] for 0.5-mm-diameter spheres at 300 K and 100 kPa. Values for thermal conductivity calculated using the adjacent pairs of thermocouples, $M1$–$M2$ and $M2$–$M3$, gave plots similar to those in Figs. 2 and 3, but with more scatter since small fluctuations in the thermocouple positions produced a larger percentage error in the calculated thermal conductivity.

5. Discussion of experimental uncertainties

Kreith [17] discusses a calculation for horizontal convection between vertical parallel plates in the absence of any vertical temperature gradients. He shows that heat flow by convection is negligible provided that the dimensionless Grashof number, Gr, is less than 8000. Gr for our beds can be estimated crudely by choosing the distance and temperature between the parallel plates in Kreith's discussion to be the average pore size between the alumina spheres and the

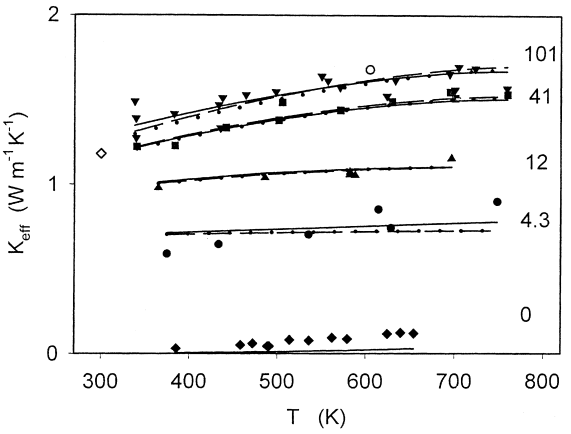

Fig. 2. Effective thermal conductivity for 1-mm alumina spheres; numbers on the figure are pressures in kPa. Solid points: experimental data of this paper. Open points: other experimental data; (◇) 0.5-mm spheres in 100 kPa He [6], (○) 1-mm spheres in 100 kPa He [7]. Lines are fits with the multiple-gap model: Solid, fitting g_{av}, B, σ, α_e, α_o, and a. Dashed, fitting g_{av} and B. Dotted, uses g_{av} and B from fit to the T = 573 K data.

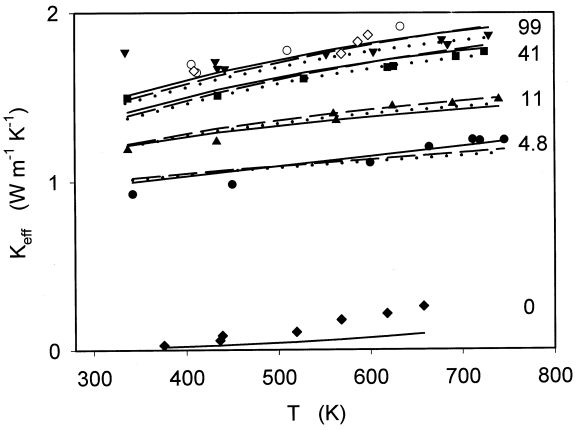

Fig. 3. Effective thermal conductivity for 3-mm alumina spheres; numbers on the figures are pressures in kPa. Solid points: experimental data of this paper. Open points: other experimental data; (○) 2-mm spheres and (◇) 4-mm spheres in 100 kPa He [7]. Lines are as in Fig. 2.

typical temperature drop across this distance. This gives $Gr \approx 7 \times 10^{-10}$, showing that convection is negligible compared to gaseous conduction.

Other sources of uncertainty in the experimental values of K_{eff} are discussed below. The possible errors from these have been summarized in Table 2. The values calculated for K_{eff} from Eq. (2) show increased uncertainty at lower temperatures because of relatively smaller values of $T(r_1)-T(r_2)$; however, the uncertainty in K_{eff} from this source drops to below 3% above 200°C.

The line voltage which powered the axial heater and heater tapes was not regulated. Toward the end of the experiments it was realized that the line voltage fluctuated as much as 3% over a period of 2 h or 5% over 6 h. A change in line voltage of 3% resulted in a change in power to the core heater of 6%. Because the response time for the cell for such a change is of the order of 3–4 h, and because most data were taken at about 9 a.m. when line voltage was changing relatively quickly, the fluctuations in line voltage resulted in an uncertainty of about 5% in calculated values of thermal conductivity.

The measured distance between the voltage taps (100 mm) could be in error by as much as 1.5 diameters of the resistance wire. This would contribute a systematic uncertainty of 2% to experimental values of K_{eff}.

Uncertainties in the measurement of the thermocouple voltages and differences in the temperature of the cold junctions (at room temperature) resulted in a maximum error of 10% in the runs near 60°C, 2% at 100°C, and less than 1% above 350°C.

The measurements of thermocouple positions were accurate to within 0.1 mm at the time that the measurements were taken. If it is assumed that the position of a thermocouple could be perturbed by 0.5 of an average sphere diameter as the bed settled, this would result in an uncertainty in thermocouple position of 0.5 mm for the smaller spheroids and 1.4 mm for the larger ones. This would lead to an uncertainty in K_{eff} of 1.5% for the 1-mm spheres and 4.3% for the 3-mm spheres for mean values of thermal conductivity calculated between $M1$ and $M3$.

In order to minimize axial heat loss from the central region of the cell by conduction through the bed along the length of the cell, the length of the axial heater was chosen to be long compared to the cell diameter. It has been shown by analysis [18] that the error due to non-radial heat flow at the cell centre, because of conduction through the ends, is less than 0.5% for a length-to-diameter ratio greater than 4. This ratio was 5.7 for the cell used in these experiments.

Computer modelling of heat flow within the experimental cell was carried out at the Canadian Centre for Fusion Fuels Technology using the ANSYS-PC/THERMAL finite element package, in the 2-D axis-

Table 2
Summary of relative errors in experimental values of K_{eff} (K_{eff} calculated from the difference in temperature between $M1$ and $M3$)

	1-mm spheres (%)		3-mm spheres (%)	
Source of error	Below 100°C	Above 100°C	Below 100°C	Above 100°C
Power	5	5	5	5
T_1-T_2	10	1	10	1
Pressure[a]	2–5	2–5	2–5	2–5
$\ln(r_1/r_2)$	2	2	4	4
Axial loss	< 1	< 1	< 1	< 1
Net error	11–13	6–8	12–13	7–8

[a] The 5% uncertainty from pressure applies only to the 10 kPa values.

symmetric mode. Results show that temperatures measured at the three mid-plane thermocouples should be within 1.5°C of the measurements that would be obtained if the cell were infinitely long. Because experimental values for thermal conductivity are calculated from the difference in temperature between thermocouples, it is concluded that the errors in these calculations due to axial heat loss are negligible. There are two potential sources of axial heat loss other than axial temperature gradients in the alumina. These are axial conduction of heat along the heater (mullite and resistance wire) and convection currents inside the mullite tube. Calculations similar to those of Ref. [1] show these to be negligible.

To provide a means of checking for axial temperature gradients experimentally, thermocouples were located above and below the midplane of the cell as discussed above. By rearranging Eq. (2) and assuming constant thermal conductivity as taken from Figs. 2 and 3, the temperature at any radial position r in the central plane of the cell can be calculated if the temperature at a specific location in the central plane r_1 is known, with

$$T(r) = T(r_1) - \frac{\dot{Q}}{2\pi l K_{\text{eff}}} \ln\left(\frac{r}{r_1}\right). \tag{4}$$

Taking $T(r_1)$ to be the temperature at $M1$, Eq. (4) was used to calculate the temperatures that would be expected at the radial positions of thermocouples $B1$, $T1$ and $B3$ if there were no axial temperature gradients. The differences between the calculated and measured temperatures at these positions were negligible, which is consistent with the finite-element analysis.

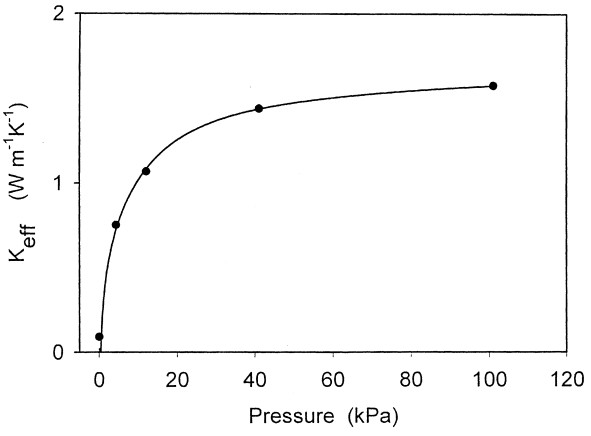

Fig. 4. Effective thermal conductivity at 573 K for 1-mm alumina spheres. Points: experimental data. Line: theoretical fit to determine g_{av} and B.

6. New theoretical model and analysis of data

6.1. Single-gap model

The main evidence for the need to include surface irregularities is seen in the data points of Fig. 4 for the 1-mm spheres, which shows K_{eff} as a function of pressure P at a constant temperature of 573 K, as interpolated from Fig. 2. A similar curve was obtained from Fig. 3 for the 3-mm spheres. The only parameter that can change under these conditions is the number density $n = P/kT$ of the gas molecules (k is Boltzmann's constant), which affects only the mean free path of the molecules given by $\lambda = (\sqrt{2} n \pi D^2)^{-1}$ [19, p.178], where D = 0.218 nm is the diameter of the He atom [20, p.266]. However, the thermal conductivity of a gas is independent of pressure when λ is much less than the average distance d between two confining surfaces. Therefore Fig. 4 clearly shows the evolution from $\lambda > d$ to $\lambda < d$ at a pressure of about 20 kPa, which corresponds to a value of λ of 1.9 μm. Since for perfectly smooth spheres the only length in the problem is the sphere radius, it is obvious that a new length scale of order 2 μm must be introduced to explain the results of Fig. 4. The most likely possibility is the depth of long-range undulations in the surface, and electron micrographs confirm they exist and have the correct order of magnitude. Note that one cannot explain the results of Fig. 4 as being due to the small gap near the point of contact for perfectly smooth spheres; for this case the area corresponding to $\lambda > d$ decreases as n increases at exactly the rate to make the conductivity in this region independent of pressure. Neither can Fig. 4 be explained by short-range roughness a few microns in height, since the narrow-gap area associated with this would generally be too small to make a significant contribution.

Some theories [5,9,10,21], have included the initial increase of K_{eff} as P is increased from zero by modelling the heat transfer per unit area per second between two parallel plates separated by a small gap d, per degree temperature difference between them, by the expression

$$K_g/(d + 2j) \tag{5}$$

where j is the temperature "jump distance" given approximately by $j = (2/a - 1)\frac{2}{\gamma+1} Pr\lambda$ [19, p. 314]. Here K_g is the gas thermal conductivity at high pressure ($\lambda << d$); the accommodation coefficient a is the energy exchange which occurs when a molecule collides with the surface, expressed as a fraction of its value for thermal equilibration. $\gamma \equiv C_P/C_V$ is the ratio of the gas heat capacities at constant pressure and volume respectively, and Pr is the gas Prandtl number ($Pr \equiv \eta C_P/K_g$) with η being the gas viscosity. For

helium, $j \sim 2\lambda$, so j is larger at low pressures. As P increases, λ decreases and the value of expression (5) increases from zero to K_g/d, giving a transition to a constant conductivity as occurs in the data points of Fig. 4. However, expression (5) is derived [5; 19, p. 314] under the assumption that there is a well defined temperature gradient in the gas between the two plates, which is true only if $d > \lambda$, and so does not apply in the case of very low pressure.

Our model assumes primitive tetragonal packing of the spheroids of average radius R, with a unit cell of area $4R^2$ perpendicular to the direction of heat flow and of length $2\alpha_e R$, as sketched in Fig. 5. Here α_e is a geometrical correction factor somewhat less than unity, to allow for the fact that the packing is expected to be denser than tetragonal. Parameter g is the average width of the gap near the points of contact between the spheres; that is, g is a measure of the depth of the surface undulations of the spheres between adjacent points of contact, and is a few μm in magnitude as discussed above, so $g << R$. The packing density is given in Table 1 as 56.7% for the small spheres and 58.0% for the large ones. This compares to values of 52.4, 68.0 and 74.0% for simple cubic, body-centred cubic and close-packed uniform spheres, respectively. Therefore, the average spacing between spheres should be close to that for simple cubic, and α_e is expected to be about $52/57 \sim 0.9$.

K_{eff} is modelled as shown in Fig. 5 in terms of thermal conductances G, where the heat flow between a temperature difference ΔT across a planar gap of width Δx and area A would be given by $\dot{Q} = KA\Delta T/\Delta x = G\,\Delta T$. This equation has the form of Ohm's law, so the conductances can be summed in the same manner as series and parallel electrical conductances.

At a pressure of 100 kPa, the conductance of an alumina sphere is significantly larger (16 to 4 times) than the sum of the conductances between adjacent spheres, as the temperature varies from 300 to 800 K. Consequently, we assume that each sphere is at a roughly constant temperature, with most of the temperature drop occurring in the gap between the spheres. This assumption becomes even more correct for pressures below 1 atm. The overall conductance can be expressed as a combination of series and parallel conductances: G_s is the relatively high conductance across the sphere, G_c is the conductance through the points of direct contact between the two spheroids, G_r is the radiation term, G_i accounts for heat flow through the gas in the "inner" gap of average width g and average radius $B \ll R$, and G_o for the gas in the "outer" gap of width of order R. If $T1$ and $T2$ are the temperatures of the mid-points of the two spheres, we can define the effective conductivity over the entire cell using

$$\dot{Q} = K_{eff} 4R^2 \frac{(T_1 - T_2)}{2\alpha_e R} = G(T_1 - T_2) \tag{6}$$

where

$$G = G_r + \frac{G_s(G_{par})}{G_s + G_{par}} \text{ with } G_{par} = G_o + G_i + G_c. \tag{7}$$

That is, G_s is in series with the parallel combination of G_o, G_i and G_c, with all this in parallel with G_r. Note that G_o has been included in parallel with G_i and G_c rather than in parallel with G_r, because the major contribution from G_o will be where the gap is the smallest. This choice provides a slightly better fit to the data than placing G_o in parallel with G_r, although clearly either is a compromise with reality; however, because G_s is so large there is little effective difference between these two choices. For the results obtained in vacuum where G_o and G_i are zero and using $G_s \gg G_c$, this becomes

$$G = G_r + G_c \tag{8}$$

to better than 1%. The individual expressions for the conductances are as follows:

$$G_s = K_s \alpha_s \pi R^2/2R,\ G_c = K_s \alpha_c \delta/h_r,$$

$$G_r = \frac{4\sigma_s}{2/\epsilon - 1}\alpha_r 4R^2 T^3,\ G_i = K_{gi}\alpha_i \pi B^2/g,$$

$$G_o = K_g[1 - \exp(-R/\lambda)]\alpha_o \pi (R^2 - B^2)/R \approx K_g[1 - \exp(-R/\lambda)]\alpha_o \pi R. \tag{9}$$

Physically, a conductance is the thermal conductivity for that mode of heat transfer, multiplied by the average value of the conduction cross-sectional area divided by the path length; hence the αs are geometrical factors of order unity. K_{gi} is the gas conductivity for λ comparable to g, as defined by Eq. (12) below. σ_S is the Stefan–Boltzmann constant, ϵ is the emissivity

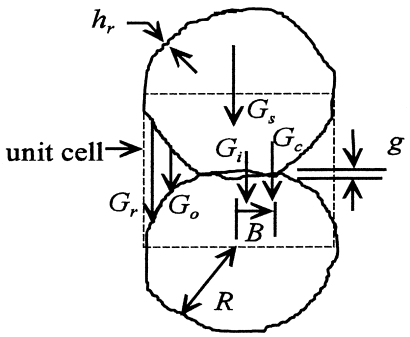

Fig. 5. Schematic for the one-gap model. The heat flow is downwards; symbols are defined in the text.

of the alumina pebble surface taken to be 0.75 [22, p. 6-157], δ is the actual area of contact between the two spheroids, and h_r is the average height of the short-range roughness and used as the length of the solid "neck" between the spheres at a contact point. K_g is the thermal conductivity of a gas when $\lambda \ll g$, namely [19, p.178]

$$K_g = \frac{25\pi}{64} n\bar{v}\lambda C_v = \frac{25\pi}{64}\bar{v}\frac{1}{\sqrt{2}\pi D^2}C_v \tag{10}$$

where C_v is the heat capacity per molecule ($3k/2$ for He), $\bar{v}=(8kT/\pi M)^{1/2}$ is the average speed of a molecule and m is its mass. The factor $1-\exp(-R/\lambda)$ in Eq. (9) removes G_o from the expression for K_{eff} when $P = 0$.

When $\lambda \gg g$, gas molecules can traverse the gap without undergoing collisions with other molecules. The thermal conductivity of the gas then becomes [19, p. 317],

$$K_{\lambda \gg g} = \frac{a}{2-a}\frac{\gamma+1}{8} n\bar{v}C_v g \tag{11}$$

where $\lambda = 5/3$ for He. Therefore, the gas thermal conductivity in the narrow gap must vary from the low-pressure limit of Eq. (11), which is linear in n, to the high-pressure limit of Eq. (10), which is independent of n, in some smooth fashion as g/λ increases as the pressure increases. Because the distance x travelled by a gas molecule without a collision varies as $\exp(-x/\lambda)$, it is reasonable to assume that the transition from $K_{\lambda \ll g}$ to K_g will depend in a similar way on the ratio of g/λ. The transition form used is given in Eq. (12), where β includes a correction for the linear dependence on n which appears at low values of n in the first term:

$$K_{gi} = K_g(1-e^{-3g/2\lambda}) + \beta g e^{-3g/2\lambda} \tag{12}$$

where

$$\beta = \left[\frac{a}{2-a}\frac{\gamma+1}{8} - \frac{3}{2}\cdot\frac{25\pi}{64}\right] n\bar{v}C_v. \tag{13}$$

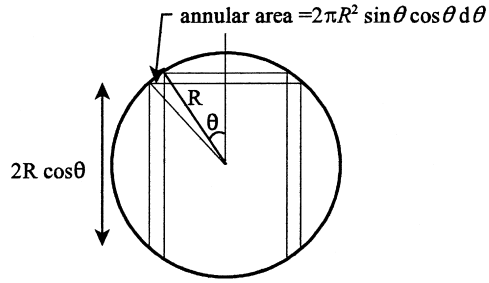

Fig. 6. Geometry for the calculation of α_s.

The factor of 2/3 in the exponent in Eq. (12) accounts for the angular dependence of the molecular paths [20, p. 264]. Note that K_g (and therefore G_o) varies as $T^{1/2}$, whereas K_{gi} (and therefore G_i) varies as $T^{-1/2}$ at low pressures and $T^{1/2}$ at high pressure. As mentioned earlier, Eq. (5) also gives the correct transition from the high- to the low-pressure limits. However, this equation was derived under the assumption that $\lambda \ll g$ which is not satisfied over most of the pressure range of interest, and it gave a substantially inferior fit to our experimental data of Fig. 4 than did Eq. (12).

We estimate $\alpha_s = 2.0$ using the geometry of Fig. 6 assuming the heat flow follows straight paths through the spheroid, by integrating the annular area divided by the path length $2\pi R^2 \sin\theta\cos\theta\,d\theta/(2R\cos\theta)$ and dividing by $\pi R^2/2R$. This value of α_s is used from now on. Similarly, we calculate α_o for conduction across the outer gap between adjacent spheroids by using Eq. (5) and integrating $2\pi R^2 \sin\theta\cos\theta\,d\theta/[2R(1-\cos\theta)+2h_r+2j]$ where θ varies from $\theta_o \sim B/R$ to $\pi/2$, and dividing by $\pi R^2/R$ to give, for $B/R \ll 1$,

$$\alpha_o = -1 - \ln\left[\frac{1}{2}\left(\frac{B}{R}\right)^2 + \frac{h_r}{R} + \frac{j}{R}\right]. \tag{14}$$

Note that it is necessary to include the roughness height h_r to prevent α_o from blowing up for small values of B and j, since the roughness will keep the gap between the two particles finite even if the long-range undulations and temperature jump distance are negligible. Since $(B/R)^2/2 \gg h_r/R$ in this paper, the term in h_r has been ignored in calculations. Using the value B = 94 μm for the small spheres (as obtained below for the 1-gap model in Table 4) and a typical value of $j \sim 3.8$ μm for He at 20 kPa and 573 K gives $\alpha_o = 2.56$ if h_r is assumed to be zero, and 2.30 if $h_r = 4$ μm. Because of the logarithmic variation, this value will change only slowly as changes in pressure and temperature vary λ. However, the calculation of Eq. (14) assumes that the pebbles remain spherical beyond their contact points separated by $2B$, and this assumption has to be evaluated when the data is fitted using measured values for g and B. Note that, although the average "outer gap" between the two spheres is $2R/3$, the value of α_o is dominated by the region of smallest gap, so that the j/R term in Eq. (14) affects the value of α_o significantly at low pressures.

We first fit the $P = 0$ curves of Figs. 2 and 3 using Eqs. (6), (8) and (9). For K_s we used a quadratic fit to experimental data for bulk alumina from the supplier in the temperature range 423–1073 K, namely $K_s = 32.7 - 0.0329T + 1.23\times10^{-6}T^2$ for material of 96% alumina (the small spheroids) and $K_s = 24.4 - 0.0341T + 1.38\times10^{-5}T^2$ for 90% alumina (the large spheroids); note that K_s decreases with tem-

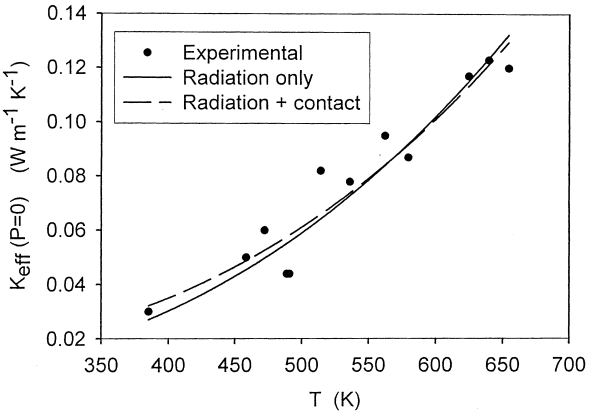

Fig. 7. Effective thermal conductivity at $P = 0$ kPa for 1-mm spheres. Points: experimental data. Lines: theoretical fits.

perature in the range of this experiment. It has been shown [21] that, even for high-density ceramics, the presence of micro-cracks can have a pronounced effect on the bulk thermal conductivity as a function of pressure. However, this should not be a serious problem here because (a) the alumina spheres are reported to be near zero porosity and (b) the conductance G_s is typically ten times $G_o + G_i$ with which it is in series, so that small changes in G_s will have little effect on the overall conductance. For the small spheres, the fit of Eq. (6) to the $P = 0$ curve produces the dashed line in Fig. 7; the solid line is the best fit assuming radiation only. A similar plot was obtained for the large spheres, except that the fitted value for G_c was totally negligible compared to G_r for the 3-mm spheres so the two lines superimposed. The values found for $\alpha_e\alpha_c\delta/h_r$ and $\alpha_e\alpha_r$ are given in Table 3; note that most of the fitted parameters in this paper are given to one more significant figure than is justified by the statistical uncertainty, in order to give the actual values used in the fits. These results show that the conduction through the points of contact is negligible compared with radiative transfer. Moreover, the uncertainties in $\alpha_e\alpha_c\delta/h_r$ make these fitted values meaningless. Therefore, the contact term G_c will be dropped from further calculations reported here. Including G_c changes these results negligibly.

The values about 3 obtained for $\alpha_e\alpha_r$ are of order unity as required, but are larger than expected given the value of 0.9 for α_e suggested earlier. A rough surface will result in an increase in the value of the emissivity in G_r and a reduction in α_r. However, even using the blackbody value of 1 reduces α_r only to 2.0. The optical transmission region for polished sapphire (which is alumina based) is 0.14–6.5 μm [22, p. 6-47], with the peak of the blackbody radiation at 500°C being 3.75 μm, so infrared transmission through the ceramic could possibly explain the discrepancy. Another possibility is that much of the thermal radiation could be reflected over several sphere diameters, significantly increasing the radiative component of heat transmission. If either of these were the causes, a value for α_r near 3 suggests that the thermal radiation travels an average distance of about three sphere diameters before being absorbed. Experiments to test this were carried out by measuring the intensity of radiation from a glow-bar held at 515°C, which was transmitted through a KBr dish containing the small spheres. KBr has a 94% transparency in the spectral range of interest. A Bomem model M100 infrared spectrometer was used as a detector, with the background transmission through the empty dish measured first. The transmitted radiation fell to approximately 10% after one layer of spheres and to about 1% after 2 layers, showing that transmission and reflection of the radiation cannot explain the large value of $\alpha_e\alpha_r$: presumably the strong scattering by grains in the spheroids makes transmission negligible. Subsequent fits to data from lithium zirconate spheroids [8,23] of similar packing fraction have given a value for $\alpha_e\alpha_r$ of 0.931 ± 0.004. If α_e for these particles is about 0.9 as estimated in the present work, this gives a value of α_r very close to 1 for the lithium zirconate work. Therefore, it is believed that the high value of α_r for the alumina spheroids is due to gas in the small gaps between particles which has diffused out of micropores in the spheroids as has been seen elsewhere (e.g. [24]), and a value of $\alpha_r = 1.0$ will be used from now on.

Parameters g and B can now be determined by fitting the data of Figs. 2 and 3 for K_{eff} to the expression obtained by substituting Eqs. (7)–(13) into Eq. (6). All curve fitting has been done with SigmaPlot 4.0, which allows simultaneous fitting of all the $P > 0$ curves. We

Table 3
Values of fitting parameters at $P = 0$

	Contact + radiation			Radiation only	
Sphere diameter	$\alpha_e\alpha_c/h_r$ (μm)	$\alpha_e\alpha_r$	R_c	$\alpha_e\alpha_r$	R_c
1-mm	0.30 ± 0.32	3.5 ± 0.2	0.957	3.7 ± 0.1	0.953
3-mm	$3 \times 10^{-8} \pm 2$	2.4 ± 0.2	0.985	2.44 ± 0.09	0.985

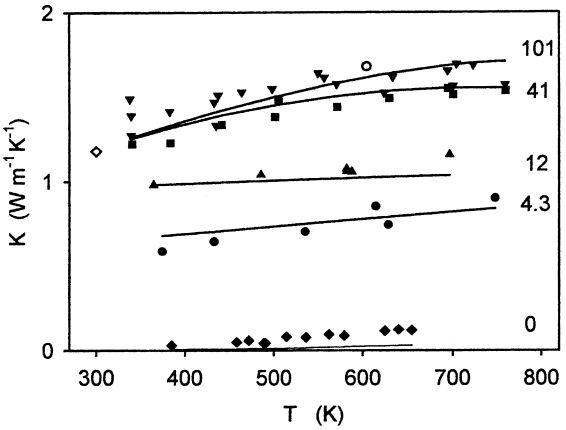

Fig. 8. Effective thermal conductivity for 1-mm alumina spheres; numbers on the figure are pressures in kPa. Points: experimental data as in Fig. 2. Lines: theoretical fit with the one-gap model.

fitted using $\alpha_s = 2.0$ as calculated above, and with $\alpha_i = 1$ since it is not separable from B^2, allowing g, B, α_e, α_o and a to vary. The results are given in Fig. 8 for the 1-mm spheres; similar results were obtained for the 3-mm spheres, with the fitted parameters listed in Table 4 under "1-gap". Here R_c is the correlation coefficient for the goodness of fit. The fitted curves agree reasonably well with the experimental data, with the major discrepancy being between the 41 and 101 kPa curves at low temperatures where the theoretical curves coalesce. Since λ is proportional to T/P, this implies that $\lambda < g$ (i.e. K_g independent of P) for both curves at low temperatures but $\lambda > g$ for the 41-kPa curve at high temperatures, and suggests that a better fit would be obtained by having a range of gap sizes which would allow for differentiation between the higher-pressure curves, as incorporated below.

6.2. Multiple-gap model

The model was modified to include a Gaussian distribution of gaps, with average gap g_{av} (corresponding to g in Eqs. (9), (11) and (12)), and standard deviation σ. The addition of σ increases the number of fitting parameters by one over the single gap model. Because SigmaPlot does not allow "loop" statements in its regressions, the distribution was divided into just eleven bins between -2σ and 2σ, centred on the average gap g_{av}. The expression for G_i for this multiple-gap model then becomes, in parallel with Eqs. (12) and (9),

$$G_{iM} = \alpha_i \pi B^2 \left\{ \sum_{j=-5}^{5} f_j \left[K_g (1 - e^{-3g_j/2\lambda}) + \beta g_j e^{-3g_j/2\lambda} \right] / g_j \right\} \quad (15)$$

where f_j is the Gaussian weighting factor for the jth bin (with $\Sigma f_j = 1$), and $g_j = g_{av} + 2\sigma j/5$; $\alpha_i \pi B^2 f_j$ is effectively the area with gap g_j. All other Gs are unchanged. The experimental data was fitted letting g_{av}, B, σ, α_e, α_o, and a vary under the constraints $B > g_{av} > \sigma > 0$, $1 \geqslant a > 0$, $1 > \alpha_e > 0$, $5 > \alpha_o > 0$. The fitted curves are shown as the solid lines in Figs. 2 and 3 for the 1-mm and 3-mm spheres, respectively, and the fitted parameters of this 5-parameter multiple-gap fit are given in Table 3 under "M-gap (5 par)".

7. Discussion of the fitted results for the 5-parameter model

Overall, the curves for the multiple-gap theory fit the experimental data well, usually within the experimental uncertainty estimated from the scatter in the

Table 4
Values of fitting parameters for $K_{eff}(T, P)$

Sphere size	Fit	g or g_{av} (μm)	σ (μm)	B (μm)	a	α_e	α_o	R_c
1-mm	1-gap	2.4 ± 0.6	–	94 ± 15	$1^a \pm 1.5$	0.80 ± 0.05	$5^a \pm 3.7$	0.969
	M-gap (5 par)	5.3 ± 1.1	2.6 ± 0.4	90 ± 13	$1^a \pm 2.8$	0.82 ± 0.18	1.8 ± 1.4	0.979
	M-gap (2 par)	4.0 ± 0.7	$g_{av}/2.06$	51 ± 6	1	0.9	Eq. (14)	0.969
	Eng. (2 par)	4.3 ± 1.2	$g_{av}/2.06$	53 ± 10	1	0.9	1	0.998[b]
3-mm	1-gap	2.0 ± 0.7	–	122 ± 19	$1^a \pm 1.9$	0.57 ± 0.08	6.4 ± 1.7	0.916
	M-gap (5 par)	5.2 ± 3.1	2.5 ± 0.9	143 ± 20	$2 \times 10^{-12} \pm 2$	0.82 ± 0.12	3.7 ± 2.5	0.970
	M-gap (2 par)	7.5 ± 1.3	$g_{av}/2.06$	130 ± 13	1	0.9	Eq. (14)	0.966
	Eng. (2 par)	7.6 ± 3.6	$g_{av}/2.06$	126 ± 36	1	0.9	Eq. (14)	0.996[b]
Xu et al.	Eng. (2 par)	4.6 ± 0.9	$g_{av}/2.06$	39 ± 9	1	0.9	Eq. (14)	0.996[b]

[a] Parameter has gone to its maximum allowed value.
[b] Fit to the He $K_{eff}(P)$ curve.

experimental points, and with correlation coefficients of about 0.97. The theory clearly incorporates the overall dependance on T and P correctly, and the values of the geometrical constants are too close to their predicted values to be accidental. The major discrepancy is with the results near 4 kPa, for which the theoretical curve has too shallow a slope for both sizes of spheres. Using the values for $\alpha_r \sim 3$ obtained from the fit at $P = 0$ kPa rather than $\alpha_r = 1$ gave a steeper slope and therefore a slightly better fit to the 4 kPa data, but fits which were too high for the high-pressure data at high temperatures. This is to be expected if the high value of α_r is due to the emission of gas from the particles, because this will have its strongest effect at low system pressures but will over-estimate the radiative T^3 conductance at high temperature. Because the assumption of multiple gaps is clearly necessary to get a reasonable fit to the data, we will restrict further discussion to this model from now on.

The values of the fitted parameters for g_{av} and B agree within a factor of 2 with rough measurements of these parameters obtained from optical photographs of the spheroids focussed on an equator, and from electron micrographs. B was estimated by drawing a straight line between successive peaks on the equator, and g_{av} as 1/3 the distance from this line to the bottom of the valley below the line. A statistical analysis of these parameters from spheroids that have been cross-sectioned, to give a clear view of the structure at the equator, is being carried out to try to eliminate the need to treat them as fitting parameters.

As might be expected from a model with five fitting parameters, the parameters are quite interdependent as indicated by values close to unity (typically 0.99) for the "dependency" value provided by the SigmaPlot regression analysis. For example, from Table 4 it is clear that the model is very insensitive to the value of the accommodation coefficient a, which always has an uncertainty greater than 100%, and which for the 1-mm spheres has gone to its upper limit of one. Its value could be altered intentionally from 0.5 to 2 with negligible change in the other fitting parameters. This is to be expected since β, which contains a, is multiplied by $g_j \exp(-1.5\ g_j/\lambda)$, so small changes in g_i can compensate for quite large changes in a. Since $a \sim 1$ for rough surfaces with multiple scattering of a gas molecule before it reaches equilibrium, we will assume this value and drop a as a fitting parameter from the model. Similarly, the values of B^2 and g_{av} might be expected to be quite interdependent, since B^2 and $g_j \exp(-1.5\ g_j/\lambda)$ are also multiplicative at low values of g_j/λ.

The theoretical model is robust. As long as SigmaPlot indicated a good convergence of the fitted curves to the experimental data, changing within reasonable limits the initial values of the parameters being fitted gave the same final results within the statistical uncertainty. Moreover, all the values for α_e and α_o are close to those expected, and only went to the limits to which they were constrained in the case of α_o for the 1-gap model. If we ignore the short-range roughness and use a typical value of $\lambda = 1.9$ μm, Eq. (14) gives a value for α_o of 2.6 and 3.8 for the small and large spheres respectively, compared to the fitted values of 1.8 ± 1.4 and 3.7 ± 2.5. These agree within the statistical uncertainty of the fitted parameters. An analysis of conductivity measurements for very smooth and spherical ball bearings would be a particularly interesting test of Eq. (14), since B should then be essentially zero.

It is interesting to look at the relative magnitudes of the conductances. For example, at 101 kPa for the 1-mm spheres, G_r, G_o, G_i, and G_s are, respectively, 4.6×10^{-6}, 6.4×10^{-4}, 7.7×10^{-3}, and 3.2×10^{-2} W K^{-1} at 338 K, and 5.2×10^{-5}, 9.5×10^{-4}, 1.0×10^{-3}, and 1.2×10^{-2} W K^{-1} at 759 K. (As has been pointed out, the value of G_c is too small and uncertain for a meaningful comparison.) This shows that G_i is the largest term in the conductivity across the gap for all temperatures and cannot be ignored in spite of the small area involved ($\pi B^2 \approx 0.04\pi R^2$). Moreover, since G_i depends strongly on irregularities in the shape of the spheroids, it is clear that a reliable estimate of the effective conductivity of packed beds cannot be made without some knowledge of these irregularities.

8. Further reduction in the number of fitting parameters

Even with the choices for a and α_r discussed above, the above model still has five fitting parameters: g_{av}, B, σ, α_e and α_o. However, the fitted curves give values of $g_{av}/\sigma = 2.04$ and 2.08 for the 1- and 3-mm spheroids, respectively. A very similar value of 2.1 has been obtained by us for both lithium zirconate [8] and beryllium spheroids [13], and values close to 2.06 have been obtained for all fits of our alumina data under slightly different versions of the theory. Therefore, we will assume a value of 2.06 is generally applicable. A value near 2 is clearly reasonable, given that one would expect a significant proportion of gaps of width near zero, and 95% of the gaps must be within 2σ of the mean value for a Gaussian distribution.

We have also shown that the fitted values of α_o agree with the results from Eq. (14) within the statistical uncertainties, so we will use this equation from now on. Finally, the values of α_e also agree with the value of 0.9 estimated from the packing density within the stated uncertainty, so we will use $\alpha_e = 0.9$ henceforth. This leaves only g_{av} and B as fitting parameters, both of which are physically measurable. Fitting all the curves except that for $P = 0$ kPa under these

assumptions yields the dashed curves of Figs. 2 and 3, and the fitted parameters labelled "M-gap (2 par)" in Table 4. There is little difference in goodness of fit between these curves and those of the 5-parameter fit, and the values of g_{av} are similar, although the fitted value of B is substantially smaller for the 2-parameter fit for the 1-mm spheroids. The "dependency" value from SigmaPlot for g_{av} and B was 0.933, which still indicates a fairly high interdependency between these two parameters. This is not surprising as discussed above, but does emphasize that even a good fit to all the data does not guarantee that the fitted parameters are the true values. It is clear that values of g_{av} and B measured directly from the spheroids must be obtained before the assumed values for the α parameters can be taken to be correct. This work is currently underway.

For engineering purposes and in the absence of unambiguous experimental values of g_{av} and B, an adequate fit often may be obtained using data collected at a single temperature, when either G_c or G_r is negligible; that is, for hard materials, or for materials at low temperatures, respectively. This would reduce considerably the amount of experimental data required to provide acceptable predictions, avoiding the long times required for the bed to reach equilibrium at a number of temperatures. This will be illustrated using the data for the 1-mm spheres at 573 K in Fig. 4. The model parameters are again only g_{av} and B. For hard materials such as alumina we can ignore conduction through the contact points, and take $\alpha_s = 2.0$, $\alpha_e = 0.9$, $a = 1$ and $\sigma = g/2.06$ as discussed earlier, and use Eq. (14) for α_o with the assumption that h_r/R is negligible. We then fit to the $K_{eff}(P)$ data at 573 K to get the fitted curve for $K_{eff}(P)$ shown for the 1-mm particles as the line in Fig. 4, and the values for g_{av} and B listed in Table 3 as the "Eng. (2 par)" results. A curve similar to that of Fig. 4 was obtained for the 3-mm spheroids, with the values obtained for g_{av} and B also listed in Table 4. These values of g_{av} and B are then used with no further fitting to generate the dotted lines in Figs. 2 and 3. There is very little difference between these curves and those obtained earlier, and they are acceptable for many purposes. The values of g_{av} and B obtained in this manner do not differ appreciably from those for the M-gap (2 par) values.

9. Comparison with other work

In this section our theoretical model has been compared with the experimental data of Xu et al. [13] for 1-mm diameter beryllium spheroids in the presence of He and N_2 gases between 30 and 40°C. This comparison is an excellent test of the model, for two reasons. First, Xu et al. have already used this data as a test bed for four different theoretical models. Second, since the same spheroids were used for both gases, once the adjustable parameters have been obtained by fitting the He data there are no free parameters to adjust for fitting to the N_2 data; only the mass, diameter and C_V per molecule must be changed. For He the latter two are 0.218 nm and $3k/2$, whereas for N_2 they are 0.376 nm and $5k/2$ [20, pp. 266, 248]. However, the experimental value for the ratio of the thermal conductivity of He gas to that of N_2 is 6.08 at atmospheric pressure [20, p. 268], whereas the theoretical ratio obtained from Eq. (10) is 4.72. Therefore we have multiplied the value for K_g from Eq. (10) by 0.777, in calculating K_{eff} for N_2. The same accommodation coefficient, $a = 1$, was used for both He and N_2. The thermal conductivity of Be at 300 K is 200 W m^{-1} K^{-1} [25].

For our fit to the He data we have set $\alpha_e = 0.9$, $\alpha_s = 2$, $\sigma = g_{av}/2.06$ and $T = 308$ K, and used Eq. (14) for α_o, in order to fit g_{av} and B. Radiation is negligible at the temperature of the experiments, so the $P = 0$ value of conductivity is due solely to contact between spheres. The original data were no longer available [26] so the data were taken from the published graphs. The uncertainty in the data for K_{eff} can be estimated from the spread in the original data points at $P = 0$ from about 0.45 to 0.55 W m^{-1} K^{-1}. We have taken the $P = 0$ point to be at 0.50 for the initial fit, giving the solid lines in Fig. 9. However, the N_2 curve is also tied to this point, so lowering the $P = 0$ value to 0.47 (which is within the limits of the experimental uncertainty) in the fit to G_c gives the results shown by the dotted lines. The resulting parameters for the best fit to the data for He are given in Table 4 under "Xu et al."

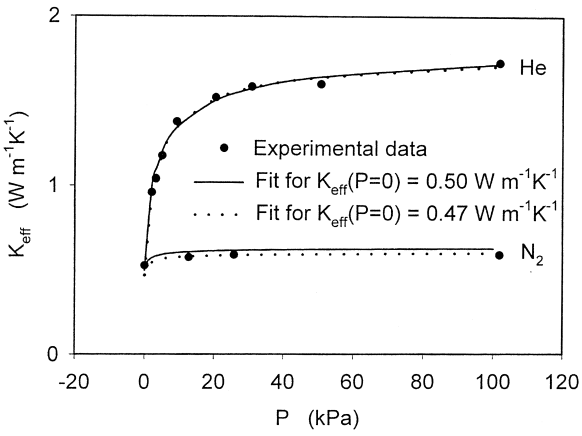

Fig. 9. Effective thermal conductivity of beryllium spheres. Large points: experimental data (Xu et al. [13]). Lines: theoretical fits.

It is seen that the beryllium data are fitted extremely well by the theory. The value of $g_{av} = 4.6$ μm is a few times larger than the value of 1–2 μm estimated [13] for the small-scale roughness, as would be expected for the undulations. Ignoring radiation means that at $P = 0$ we have

$$K_{eff}(0) = \alpha_e G_c/2R = \alpha_e \alpha_c K_s(\pi r_c^2/h_r)/2R, \quad (16)$$

where r_c is the average radius of the contact area and h_r/α_c is the average length of the contact. Equating Eq. (16) to the experimental value of 0.47 and using $h_r = 1$ μm as estimated [13], gives $(r_c/R)^2 \sim 3.3 \times 10^{-6}$, for α_c set equal to one. This is less than the maximum limit of 10^{-5} considered to be acceptable by Xu et al. [13] and so is a reasonable value. The present fits are better than those by any of the models considered by Xu et al., although it is difficult to give a full comparison without knowing exactly how many adjustable parameters Xu et al. used in their fits.

Excellent fits with reasonable parameters have also been obtained [23] for data [8] on lithium zirconate spheroids at temperatures up to 1600 K, at which temperature the radiative contribution to the thermal conductivity is at least as important as the other contributions. The model can also explain the rather surprising observation that various packed beds of 1-mm-diameter spheroids in 100 kPa of helium gas, consisting of many different materials with likely quite different surface textures, (e.g. [15]) have thermal conductivities which are very comparable in magnitude, between about 1.3 and 2.5 W m^{-1} K^{-1}, even though the bulk conductivities of the solid vary over a much wider range than this. First, it is clear why the thermal conductivity is largely independent of the material: if the conductance G_s of the solid is much greater than G_r, G_c, G_o or G_i, then the total conductance G in Eq. (6) is essentially independent of G_s. Moreover, if G_c is negligible compared to $G_o + G_i$, as will generally be the case except at low pressure because of the very small contact area, then the overall conductance will depend only on G_r and $G_o + G_i$, with G_r being small for temperatures less than 1000 K as in the cases being considered [15]. Thus the bulk conductivity has been eliminated as a major factor in the bed conductivity. It is now useful to look at the variation of G_o and G_i as B and g_{av} are changed, for the alumina spheroids. For values of (g_{av}, B), in microns, of (4.3, 53), (1, 10), and (0.1, 1), the "Eng. (2 par)" fit to the 1-mm spheroids gives values of (G_o, G_i) in units of 10^{-3} W m^{-1} K^{-1} of (0.95,1.0), (1.76, 0.061), and (1.83, 0.00058), respectively. That is, the value of G_o increases only slowly as g_{av} and B are decreased, because from Eq. (14) the value of α_o depends only logarithmically on B^2 (and even more weakly for $B^2/R < j$), whereas G_i varies directly as B^2 and so becomes quickly negligible, with their sum changing only little from 1.96 to 1.83 for the three situations considered here. It is reasonable to assume that $B \leqslant 0.1R$ and $g_{av} \leqslant 0.1B$ for a particle to be referred to as "spherical", so these results for alumina are likely to remain qualitatively true for other spheroids as well.

10. Conclusions

The effective thermal conductivity has been measured for packed beds of alumina spheroids in static helium gas from 0 to 100 kPa and 100 to 500°C. These results are in good agreement with results by other authors at a few discrete temperatures and 100 kPa. A new theoretical model for packed beds of spheroidal particles has been developed which incorporates measurable parameters for those gaps between particles which are comparable in width to the mean free path. Such gaps must exist between irregularly shaped spheroids and, although small in area, can dominate the conduction across the gaps. When a distribution of such gaps is incorporated into the model, an excellent fit to experimental data over a wide range of temperature and pressure is obtained with a relatively small number of well defined physical parameters, all of which attain reasonable values. The fits remain good when the number of adjustable parameters is reduced to two, the average width and radius of the small gaps between particles, although the assumptions remain to be tested using measurements of these parameters on actual particles. It is shown that a satisfactory approximation may be obtained by using data taken at a single temperature, for a range of pressures. The model also fits other published data well.

Acknowledgements

The authors gratefully acknowledge the contributions made to this project by Ken Fowler for his technical expertise; Dave Marshall for his assistance in taking measurements; Eldon Puckrin for the infrared measurements; Paul Gierszewski, John Earnshaw and Michael Robinson for many useful discussions; and the Fusion Fuels Technology Programme for its finite-element analysis. Financial assistance from CFFTP and the National Science and Engineering Research Council of Canada is much appreciated. JH acknowledges receipt of an NSERC Undergraduate Summer Research Award during part of this work.

Note added in proof. Subsequent modelling of other materials [23] has shown the Eq. (7) is better written as

$G = G_r + G_o + \frac{G_s G_{par}}{G_s + G_{par}}$, where $G_{par} = G_i + G_c$. This change has a negligible effect on the current paper.

References

[1] F.A. Londry, A.J. Slavin, Thermal conductivity of a packed bed of hollow zirconia microspheres, under vacuum and under 100 kPa of argon, J. Am. Ceramic Soc. 74 (1991) 3118–3125.

[2] D.L. McElroy, D.W. Yarbrough, G.L. Copeland, F.J. Weaver, R.S. Graves, T.W. Tong, H.A. Fine. Development of advanced thermal insulation for appliances, Oak Ridge National Laboratory Report ORNL/CON-159 1984.

[3] J.D. Sullivan, C.L. Brayman, R.A. Verrall, J.M. Miller, P.J. Gierszewski, F. Londry, A. Slavin, Canadian ceramic breeder sphere-pac technology: capability and recent results, Fusion Eng. Des. 17 (1991) 79–95.

[4] M.G. Freiwald, W.R. Paterson, Accuracy of model predictions and reliability of experimental data for heat transfer in packed beds, Chem. Eng. Sci. 47 (1992) 1545–1560.

[5] D.U. Ringer, Heat transfer across small gaps, in: S. Mujumdar (Ed.), Drying of Solids, Wiley (Halstead Press), New York, 1986, pp. 84–90.

[6] D.L. McElroy, F.J. Weaver, M. Shapiro, A.W. Longest, D.W. Yarbrough, The thermal conductivity of beds of spheres, in: D.P.H. Hasselman, J.R. Thomas Jr (Eds.), Thermal Conductivity 20, Proceedings of the 20th Int. Thermal Conductivity Conf., Plenum, New York, 1989, pp. 423–433.

[7] G. Sordon. Über den Wärmetransport in Kugelschüttungen, Report KfK 4451 EUR 11391DE, Kernforschungzentrum Karlsruhe GmbH, Karlsruhe 1988.

[8] J.W. Earnshaw, F.A. Londry, P.J. Gierszewski, The effective thermal conductivity of a bed of 1.2-mm-diam. lithium zirconate spheres in helium, Fusion Technol. 33 (1998) 31–37.

[9] R.O.A. Hall, D.G. Martin, The thermal conductivity of powder beds. A model, some measurements on UO_2 vibro-compacted microspheres, and their correlation, J. Nucl. Mater. 101 (1981) 172–183.

[10] R. Bauer, E.U. Schlünder, Effective radial thermal conductivity of packings in a gas flow. Part II, Thermal conductivity of the packing fraction without gas flow, Int. Chem. Eng. 18 (1978) 189–204.

[11] E. Tsotsas, H. Martin, Thermal conductivity of packed beds: a review, Chem. Eng. Process. 22 (1987) 19–37.

[12] W. Fundamenski, P. Gierszewski, Heat transfer correlations for packed beds, Fusion Technol. 21 (1992) 2123.

[13] M. Xu, M.A. Abdou, A.R. Raffray, Thermal conductivity of a beryllium gas packed bed, Fusion Eng. Des. 27 (1995) 240–246.

[14] P. Adnani. Modeling of transport phenomena in porous media, PhD thesis, University of California, Los Angeles, CA, 1991.

[15] M. Enoeda, K. Furuya, H. Takatsu, S. Kikuchi, T. Hatano, Effective radial thermal conductivity measurements of the binary pebble beds by hot wire method for the breeding blanket, Fusion Technol. 34 (1998) 877.

[16] P. Adnani, I. Catton, A.R. Raffray, M.A. Abdou, Effective thermal conductivity of binary mixtures at high solid to gas conductivity ratios, Chem. Eng. Comm. 120 (1993) 45–58.

[17] F. Kreith, Principles of Heat Transfer, International Textbook Company, Scranton, PA, 1958, p. 318.

[18] G.A. Slack, C. Glassbrenner, Thermal conductivity of germanium from 3°K to 1020°K, Phys. Rev. 120 (1960) 782–789.

[19] E.H. Kennard, Kinetic Theory of Gases, McGraw-Hill, New York, 1938.

[20] F.W. Sears, An Introduction to Thermodynamics, the Kinetic Theory of Gases, and Statistical Mechanics, 2nd ed., Addison-Wesley, Reading, MA, 1952.

[21] E. Litovsky, T. Gambaryan-Roisman, M. Shapiro, A. Shavit, Heat transfer mechanisms governing thermal conductivity of porous ceramic materials, Trends in Heat, Mass and Momentum Transfer 3 (1997) 147–167.

[22] D.W. Gray (Ed.), American Institute of Physics Handbook, 2nd ed., McGraw-Hill, New York, 1963.

[23] A.J. Slavin, To be published.

[24] E.Ya Litovskii, F.S. Kaplan, A.V. Klimovich, Effect of physicochemical processes in fireproof materials on thermal conductivity, J. Eng. Phys. 33 (1977) 813–818.

[25] C. Kittel, Introduction to Solid State Physics, 5th ed., Wiley, New York, 1976, p. 126.

[26] M.A. Abdou, Personal communication, UCLA, 1998.